Z. Phys. C – Particles and Fields 47, 367–375 (1990)

Zeitschrift für Physik C Particles and Fields
© Springer-Verlag 1990

Transverse momentum distributions of neutral pions from central and peripheral $^{16}O + Au$ collisions at 200 $A \cdot$GeV

WA 80 Collaboration

R. Albrecht[1], T.C. Awes[5], C. Baktash[5], P. Beckmann[4], F. Berger[4], R. Bock[1], G. Claesson[3], G. Clewing[4], L. Dragon[4], R.L. Ferguson[5], A. Franz[5,b], S. Garpman[3], R. Glasow[4], H.Å. Gustafsson[3], H.H. Gutbrod[1], K.H. Kampert[4], B.W. Kolb[1], P. Kristiansson[3], I.Y. Lee[5], H. Löhner[4,a], I. Lund[1], F.E. Obershain[5,b], A. Oskarsson[3], I. Otterlund[3], T. Peitzmann[4], S. Persson[3], F. Plasil[5], A.M. Poskanzer[2], M. Purschke[4], H.G. Ritter[2], R. Santo[4], H.R. Schmidt[1], T. Siemiarczuk[1,c], S.P. Sørensen[5,b], E. Stenlund[3], G.R. Young[5]

[1] Gesellschaft für Schwerionenforschung (GSI), D-6100 Darmstadt, Federal Republic of Germany
[2] Lawrence Berkely Laboratory, Berkeley, CA 94720, USA
[3] University of Lund, S-22362 Lund, Sweden
[4] University of Münster, D-4400 Münster, Federal Republic of Germany
[5] Oak Ridge National Laboratory, Oak Ridge, TN 37831, USA

Received 26 February 1990

Abstract. The production of neutral pions by the interaction of 200 $A \cdot$GeV p and ^{16}O projectiles with a Au target has been studied in the pseudorapidity range $1.5 \leq \eta \leq 2.1$. Transverse momentum spectra have been measured between 0.4 GeV/c and 3.6 GeV/c and their dependence on the centrality of the collision has been investigated. The peripheral-collision spectra display a marked change of slope with a hard component starting at about 1.8 GeV/c, in contrast to central-collision data. The data are discussed in comparison to p+p and $\alpha+\alpha$ data from the ISR.

1 Introduction

First results from ultrarelativistic heavy-ion experiments at the CERN SPS [1] have shown that with 200 $A \cdot$GeV ^{16}O projectiles on heavy targets, high energy densities are created, which approach the critical values for a quark gluon phase transition predicted by QCD lattice calculations [2]. One means of studying the properties of the compressed and highly excited reaction zone is the investigation of p_T spectra of produced pions and their dependence on the centrality of the reaction. To distinguish different contributing processes and to provide a reliable basis for comparisons with p+p scattering, a large p_T converage is required. In particular, data at high p_T values, where hard processes become important and may be calculated by perturbative QCD are of great interest. The present investigation of π^0 spectra has, therefore, concentrated on detailed measurements of p_T spectra up to 3.6 GeV/c and on selections of the data according to the centrality of the reaction. Results presented here cover the full data set of the 1986 ^{16}O + Au run and extend the subset of data previously published in [3].

2 Experimental setup and trigger requirements

The experiment has been performed at the CERN SPS using the WA80 setup [4] schematically shown in Fig. 1. The data were obtained by means of an electromagnetic calorimeter (SAPHIR), a uranium scintillator sampling calorimeter located at zero degree (ZDC), an iron scintillator calorimeter located at mid-rapidity (MIRAC), streamer tube multiplicity arrays (LAM, MIRAM, SAM), and the Plastic Ball located in the target fragmentation region.

The ZDC measures the forward energy distribution ($\eta \geq 6.0$) which is dominated by projectile spectators. It has been found [5] that the ZDC energy E_{ZDC} for ^{16}O + Au can be related to the number of participants and,

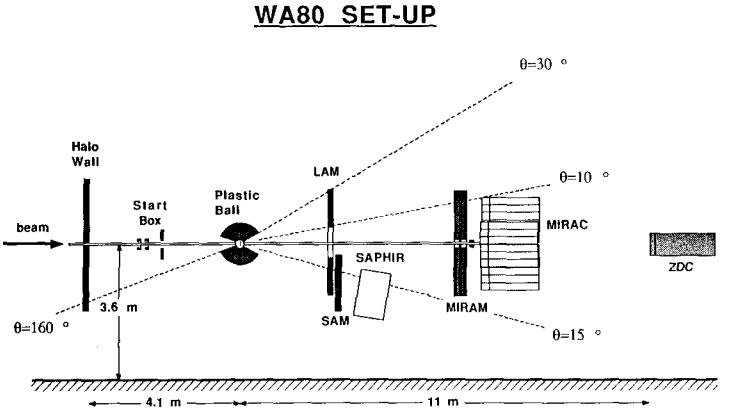

Fig. 1. Schematic view of the WA80 setup.
The different abbreviations are explained in the text

[a] now at: KVI, University of Groningen, NL-9747 AA Groningen, Netherlands
[b] University of Tennessee, Knoxville, TN 37996, USA
[c] On leave of absence from the Inst. of Nuclear Studies, PL-00681 Warsaw, Poland

hence, is a measure of the centrality of the reaction. The total transverse energy in the pseudorapidity range $2.4 \leqq \eta \leqq 5.5$ is measured by MIRAC. LAM, MIRAM and the Plastic Ball, together cover 97% of 4π sr solid angle and provide the total number of charged particles per event. It has been shown that the ZDC energy, the total transverse energy, and the number of charged particles are strongly correlated [5, 6]. Any of the three quantities can, therefore, be used for event characterization.

In our setup the minimum-bias trigger is defined by the requirements that:

- less than 88% of the total projectile energy is deposited in the ZDC (for ^{16}O beams but not for p beams);
- at least one charged particle is recorded by LAM or MIRAM ($1.2 \leqq \eta \leqq 4.4$).

In the following, central 200 $A \cdot$GeV ^{16}O+Au events are defined by $0\% \leqq E_{ZDC}/E_{beam} \leqq 30\%$, corresponding to 37% of the minimum-bias cross section σ_{mb}, while peripheral events are defined by $40\% \leqq E_{ZDC}/E_{beam} \leqq 88\%$ (54% of σ_{mb}). In a geometrical picture these cuts imply that in central events all projectile nucleons participate in the reaction whereas only a part of the projectile interacts in peripheral reactions.

The lead-glass detector, SAPHIR, is located at a distance of 342 cm from the target and covers about 1/6th of the azimuth φ in the pseudorapidity range $1.5 \leqq \eta \leqq 2.1$ corresponding to a lab. angle $13.7° \leqq \theta \leqq 25.9°$. The SAPHIR detector consists of 1278 SF5 lead-glass blocks. The dimensions of one block are $35 \times 35 \times 460$ mm^3 equivalent to 18 radiation lengths ($X_0 = 25.5$ mm). Each block is wrapped in a double layer of 10 μm aluminium-coated mylar foil in order to prevent optical crosstalk, and is equipped with a 10-stage photomultiplier [7]. The average gain stability of the module, monitored during beam time by a laser reference system, was found to be better than 0.5%. Each of the modules had been calibrated with an electron beam at the CERN SPS.

The calorimeter energy resolution was measured with an electron beam at DESY, and is described by:

$$\frac{\sigma}{E} = 0.4\% + \frac{6\%}{\sqrt{E/\mathrm{GeV}}}. \tag{1}$$

At 10 GeV/c a position resolution of 5 mm for an angle of incidence of 15 degrees was obtained by comparing the reconstructed shower position with the electron position measured by a delay line wire chamber. The observed π^0 and η mass resolution during the operation of the calorimeter at the CERN SPS was slightly worse than expected from the calibration data mainly due to the effect of overlapping showers in the high particle multiplicity environment of heavy ion reactions. An effective energy resolution of $\sigma/E \approx 8.6\%/\sqrt{E/\mathrm{GeV}}$ and $\sigma_x \approx 5.9$ mm at 10 GeV/c is obtained by a fit to the experimental data.

3 Data analysis

Electromagnetic showers deposit their energy into more than one module depending on energy, angle of incidence and hit position relative to the module boundaries. Such a group of adjacent modules with a signal above threshold will in the following be called a *cluster*. With the information of the streamer tube arrays LAM and SAM in front of SAPHIR the clusters are assigned to charged or neutral. In addition, the clusters are compared with the calculated response of electromagnetic showers [8] necessary to separate possible overlapping showers within one cluster. The efficiency of this procedure will be discussed in the next section.

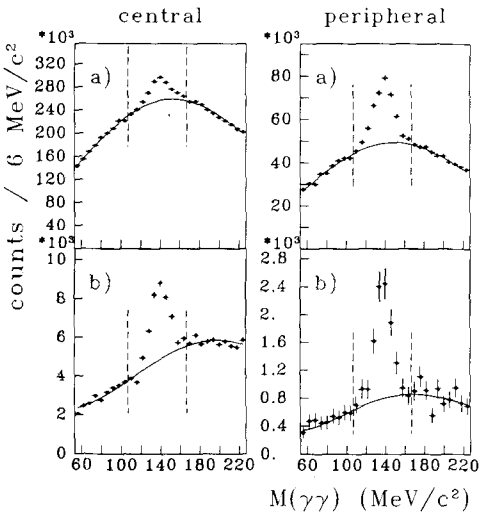

Fig. 2a, b. Invariant mass spectra for peripheral and central 200 $A \cdot$GeV ^{16}O+Au reactions and polynomial background fits in the p_T bins: **a)** 0.6 GeV/c $\leqq p_T \leqq$ 0.8 GeV/c, **b)** 1.4 GeV/c $\leqq p_T \leqq$ 1.6 GeV/c. The dashed lines indicate the π_0 peak region used for integration

Transverse momentum distributions of neutral pions, which are identified by their decay photons ($\pi^0 \to 2\gamma$), are obtained by accumulating invariant mass spectra for different bins of $\vec{p}_T = \vec{p}_T(\gamma_1) + \vec{p}_T(\gamma_2)$ (Fig. 2). In this analysis, only neutral showers with an energy above 500 MeV are used. In order to determine the π^0 peak area in each invariant mass spectrum, a polynomial is fitted to the combinatorial background and subtracted from the spectrum. The π^0 peak area is then integrated from 107 MeV/c^2 to 167 MeV/c^2 which corresponds to 99.7% of the area assuming a gaussian function with a standard deviation of 10 MeV/c^2. The uncertainty σ_N in determining the number N of neutral pions in a p_T bin is determined by statistics and the peak to total ratio Q [9]:

$$\sigma_N = \sqrt{\frac{2N}{Q} - N}. \tag{2}$$

In Fig. 2 invariant mass spectra are displayed from central and peripheral 200 $A \cdot$GeV ^{16}O+Au reactions in two different bins of p_T. They show the typical behaviour of Q, which is determined by the photon density in phase space:

1. Q increases with increasing transverse momentum,
2. Q decreases with increasing photon multiplicity i.e. at the same p_T interval Q is higher in peripheral than

Table 1. Number of analyzed events N_{events} and reconstructed π^0

System		N_{events} ÷1000	Reconstructed π^0 ÷1000
200 GeV p+Au		572	11
200 A·GeV O+Au			
Minimum-bias	$(0\% \leqq E_{ZDC}/E_{beam} \leqq 88\%)$	2204	264
Central	$(0\% \leqq E_{ZDC}/E_{beam} \leqq 30\%)$	1730	229
Peripheral	$(40\% \leqq E_{ZDC}/E_{beam} \leqq 88\%)$	344	23

in central collisions. The mean number of neutral hits with an energy above 500 MeV increases from 2.1 for peripheral collisions to 5.1 for central reactions.

The final number ΔN_{corr} of π^0 emitted into SAPHIR's solid angle in a given Δp_T is obtained by correcting the measured number ΔN with the geometrical acceptance and the γ reconstruction efficiency described in the next section.

The invariant π^0 cross section $E d^3\sigma/dp^3$ is calculated by the following expression:

$$\frac{\sigma_{mb}}{N_{events}\Delta\eta\Delta\varphi p_T}\frac{\Delta N_{corr}}{\Delta p_T}. \tag{3}$$

Here N_{events} is the number of analyzed events given in Table 1. As the absolute invariant π^0 cross sections are not discussed in the following, the uncertainty of $\sigma_{mb}(\pm 10\%)$ [10] is not taken into account in the error calculation and no attempt has been made to calculate the efficiency of the minimum-bias trigger conditions or to extrapolate the minimum-bias cross section to the total inelastic cross section. In the considered p_T range the pseudorapidity interval $\Delta\eta$ is used instead of the rapidity interval which introduces a maximum relative error of only 0.5%.

The absolute energy scale and its linearity can be monitored by investigating the π^0 mass peak position as a function of the energy of one photon, the other photon energy fulfilling the constraint $0.8\ \text{GeV} \leqq E_\gamma \leqq 2\ \text{GeV}$ (see Fig. 3). Any nonlinearity should then be visible as a shift of the π^0 peak position with varying photon energy. The π^0 peak position μ (solid circles), which is fitted by a gaussian turns out to be nearly independent of the photon energy. A maximum nonlinearity in $\Delta E/E$ of 3% can be derived from the experimental data. However, the mean peak position increases from $136.6 \pm 0.2\ \text{MeV/c}^2$ for minimum-bias 200 GeV p+Au reactions to $138.4 \pm 0.2\ \text{MeV/c}^2$ for minimum-bias 200 A·GeV ^{16}O+Au reactions. The mean number of photons with an energy above 500 MeV for the two systems is 0.5 and 4.7, respectively, which leads for the 200 A·GeV ^{16}O+Au events to a higher probability that two or more showers merge to one. This tends to increase the energy of the shower and yields a higher mass of the reconstructed π^0 and an asymmetric shape of the mass peak. In order to account for this effect, an modified gaussian with the following parametrization is applied:

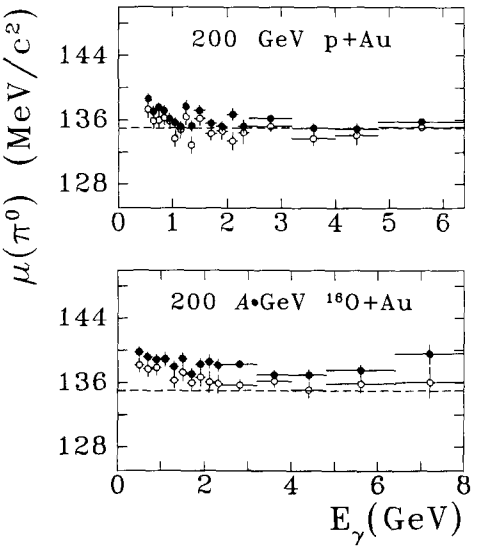

Fig. 3. Position μ of the π^0 peak as a function of one photon energy (solid circle) obtained by fits of a polynomial plus a gaussian to the invariant mass spectra. Results obtained by using an modified gaussian are also shown (definition see text, open circles). One photon energy is constrained to the interval $0.8\ \text{GeV} \leqq E_\gamma \leqq 2\ \text{GeV}$

$$f(x) = \begin{cases} A \exp\left(\dfrac{-0.5\,\omega^2}{1+\beta\omega}\right) & \text{for } x \geqq \mu \\ A \exp(-0.5\,\omega^2) & \text{for } x < \mu \end{cases}$$

$$\omega = \frac{x-\mu}{\sigma}. \tag{4}$$

Here x is the invariant mass, A the normalization constant and β the asymmetry parameter. For the 200 A·GeV ^{16}O+Au events and a photon energy above 2 GeV these peak positions (open circle in Fig. 3) agree with the rest mass.

The mass shift from the system p+Au to the system ^{16}O+Au causes a maximum relative change of the $\Delta N/\Delta p_T$ distribution of 20%. The $\pi^0 p_T$ distributions are corrected for this effect. The relative uncertainty of the corrected $\Delta N/\Delta p_T$ is estimated by Monte Carlo Simulations to be smaller than 4%.

4 Efficiency and acceptance corrections

As mentioned before, the efficiency to identify a hit as a photon is determined by the probability ε_γ to assign it as a neutral particle and the probability κ that no overlap with unresolved nearby showers has occurred. Both quantities are found to be multiplicity dependent. In the following we will discuss them as a function of the mean mulitplicity μ_{all} of all hits, which are determined for different classes of events. In this context hit means the number of resolved particles implying that one cluster may consist of two hits whose centroids could still be distinguished.

The probability that a photon is correctly identified as a neutral particle can be determined by calculating the invariant mass for pairs of one neutral particle, called *trigger particle*, combined with all other particles in the same event. In order to increase the probability to recon-

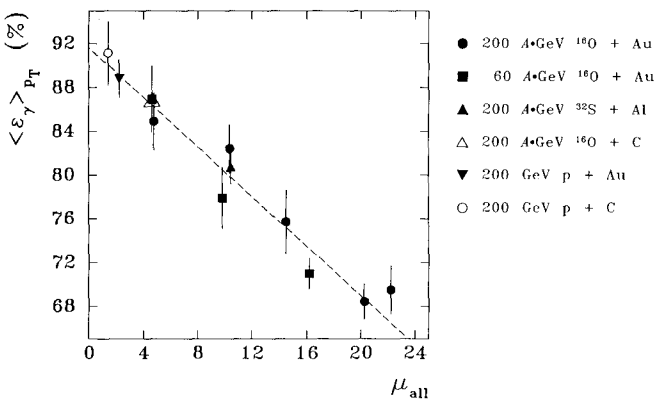

Fig. 4. Probability ε_γ (see (5)) averaged over p_T as a function of the mean multiplicity of hits μ_{all} for different reaction systems and centralities of the reactions

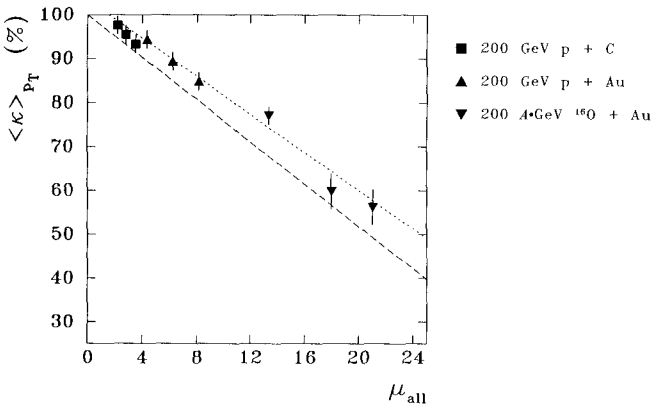

Fig. 5. Probability κ (see text) averaged over p_T as a function of the mean multiplicity of hits μ_{all}. The different points for one reaction system are calculated by superimposing two, three, and four events. The two lines represent the estimated systematic uncertainty of the probability

struct a π^0, the trigger particles γ_t have been chosen from those neutral particles which are very similar to the calculated response of an electromagnetic shower and which possess an energy above 400 MeV. For 100% reconstruction probability a π^0 peak should appear only in the mass spectrum filled by the γ_t+neutral particle combination. With the very realistic assumption that the photon identification is independent of the origin of the photon, the probability ε_γ is determined by the ratio of the π^0 peak areas A taken from the two mass spectra with particle combinations γ_t+neutral particle and γ_t +charged particle, respectively,

$$\varepsilon^\gamma(p_T) = \frac{A_{\text{neutral}}(p_T)}{A_{\text{neutral}}(p_T) + A_{\text{charged}}(p_T)}. \tag{5}$$

In this formula p_T is the transverse momentum of the charged or neutral particle. For the analyzed data no significant p_T dependence is found for ε_γ [11]. In Fig. 4 the mean probability $\langle \varepsilon_\gamma \rangle$ p_T averaged over p_T is plotted as a function of the mean multiplicity μ_{all}. Photon conversion in the material in front of SAPHIR (vacuum chamber, streamer tubes and the target itself) limits the theoretical maximum efficiency to 94% in case of a 250 mg/cm^2 Au target. This value is nearly reached for low multiplicity events, however, due to the higher probability for accidental assignment of a photon as a charged particle, $\langle \varepsilon_\gamma \rangle_{p_T}$ drops from 90% at $\mu_{all}=1.4$ to 68% at $\mu_{all}=21.1$.

The influence of overlapping showers not resolved by this analysis is determined by superimposing raw data events with low particle multiplicity and comparing the particle identification from the superimposed events with the identification of the low particle multiplicity events. Again no significant p_T dependence is found for the probability κ, except for the superimposed events with the highest mulitplicity, $\mu_{all}=21.1$. Figure 5 displays $\langle \kappa \rangle_{p_T}$ as a function of the mean multiplicity μ_{all}. Starting with minimum-bias 200 GeV p+C, 200 GeV p+Au and peripheral 200 $A\cdot$GeV ^{16}O+Au reactions the synthetic events are created by superimposing two, three and four of these events. The region between the two lines in Fig. 5 demonstrates the estimated systematic uncertainty of this procedure which is caused by the fact that even peripheral 200 $A\cdot$GeV ^{16}O+Au events do have a mean mulitplicity of $\mu_{all}=7$ and therefore already contain a certain number of overlapping showers which can not be resolved.

In order to obtain the total γ reconstruction efficiency both probabilities, $\varepsilon_\gamma(p_T)$ and $\kappa(p_T)$, have to be multiplied and in the case that both quantities are independent of p_T, one may use the product of $\langle \varepsilon_\gamma \rangle_{p_T}$ and $\langle \kappa \rangle_{p_T}$.

The total acceptance for assigning both decay photons as resolved neutral particles is calculated by a Monte Carlo simulation taking into account:

i) branching ratio for the decay $\pi^0 \to 2\gamma$,
ii) π^0 angular distribution from the event generator FRITIOF [12],
iii) a maximum nonlinearity of $\Delta E/E = 3\%$,
iv) an uncertainty of ± 50 MeV for the software energy threshold of 500 MeV due to finite energy resolution,
v) the total γ reconstruction efficiency,
vi) a minimum opening angle of 0.95° necessary to resolve two π^0 decay photons.

Figure 6 shows the total acceptance for peripheral and central 200 $A\cdot$GeV ^{16}O+Au reactions. The magnitude of the errors, which are added quadratically, is displayed as the shaded areas in Fig. 6. The main contribution stems from the uncertainty of the total γ reconstruction efficiency, whereas the nonlinearity and the uncertainty of the energy threshold do have minor influence on the total error. Furthermore, it has been verified that the acceptance is insensitive to the details of the angular distribution used in this calculation. The minimum opening angle for the π^0 decay photons influences the acceptance at $p_T \geqq 4$ GeV/c. This effect is responsible for the drop of the acceptance in Fig. 6a).

The reliability of the p_T dependence of the acceptance calculation has been checked by comparing distributions of the energy asymmetry α:

$$\alpha = \frac{|E_1 - E_2|}{E_1 + E_2} \tag{6}$$

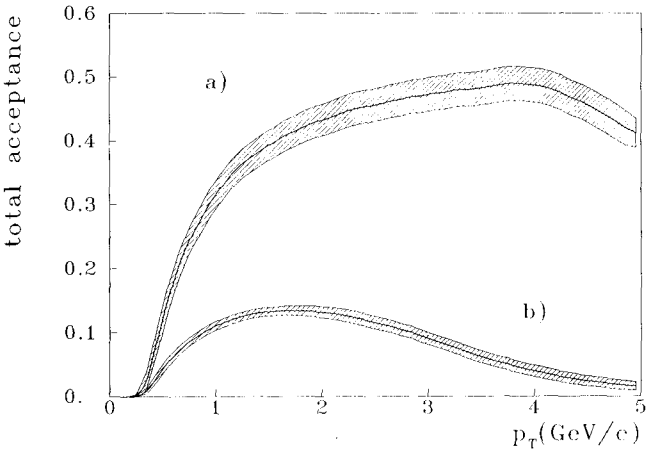

Fig. 6. Total acceptance for measuring both decay photons from π^0 with transverse momentum p_T as neutral resolved particles for *a*) peripheral and *b*) central 200 $A\cdot$GeV ^{16}O+Au reactions. The shaded area represents the total error (description see text)

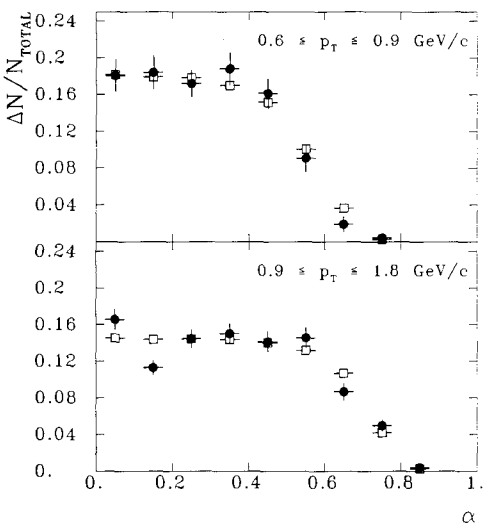

Fig. 7. Energy asymmetry α for central 200 $A\cdot$GeV ^{16}O+Au events for two p_T bins (solid circles). For comparison the Monte Carlo results are shown (squares)

from experimental data with those from a Monte Carlo calculation. Here E_1, E_2 are the energies of the π^0 decay photons. Figure 7 shows results for central 200 $A\cdot$GeV ^{16}O+Au reactions. The distributions agree within the statistical errors with the Monte Carlo calculations. Hence it can be concluded from the region above $\alpha \approx 0.5$ that the detector geometry and energy cut is well implemented in the Monte Carlo simulation and from α below 0.2 that the merging of high energetic decay photons does not occur in the p_T region under consideration.

5 Results and discussion

Invariant π^0 cross section for reactions of p and ^{16}O projectiles with a Au target at 200 $A\cdot$GeV have been obtained as a function of transverse momentum for different trigger conditons. The experimental cross-sections are given in Tables 2–5. In Fig. 8 minimum-bias data for p+Au are compared to charged pion cross sections from Ref. [13]. In the overlap region there is excellent agreement between the different data sets. An exponential which describes the pion p_T distribution below p_T

Table 2. Invariant cross-section for the reaction 200 GeV p+Au, obtained with minimum bias trigger conditions

p_T range (GeV/c)	$E(d^3\sigma/dp^3)$ (mb c^3 GeV^{-2})
0.4–0.5	$(1.2\pm0.3)\times10^3$
0.5–0.6	$(5.8\pm0.9)\times10^2$
0.6–0.7	$(2.8\pm0.3)\times10^2$
0.7–0.8	$(1.8\pm0.2)\times10^2$
0.8–0.9	$(1.1\pm0.1)\times10^2$
0.9–1.0	$(6.3\pm0.6)\times10^1$
1.0–1.1	$(3.4\pm0.3)\times10^1$
1.1–1.2	$(2.1\pm0.2)\times10^1$
1.2–1.3	$(1.3\pm0.1)\times10^1$
1.3–1.4	$(9.4\pm1.0)\times10^0$
1.4–1.5	$(4.6\pm0.6)\times10^0$
1.5–1.6	$(2.8\pm0.5)\times10^0$
1.6–1.7	$(1.7\pm0.3)\times10^0$
1.7–1.8	$(1.1\pm0.2)\times10^0$
1.8–1.9	$(6.8\pm1.8)\times10^{-1}$
1.9–2.0	$(5.4\pm1.5)\times10^{-1}$
2.0–2.2	$(2.9\pm0.7)\times10^{-1}$
2.2–2.4	$(8.4\pm3.4)\times10^{-2}$
2.4–2.8	$(2.2\pm1.2)\times10^{-2}$
2.8–3.2	$(7.7\pm6.3)\times10^{-3}$

Table 3. Invariant cross-section for the reaction 200 $A\cdot$GeV ^{16}O +Au, obtained with minimum bias trigger conditions

p_T range (GeV/c)	$E(d^3\sigma/dp^3)$ (mb c^3 GeV^{-2})
0.4–0.5	$(4.2\pm1.0)\times10^4$
0.5–0.6	$(1.6\pm0.2)\times10^4$
0.6–0.7	$(8.7\pm1.0)\times10^3$
0.7–0.8	$(5.4\pm0.5)\times10^3$
0.8–0.9	$(3.3\pm0.3)\times10^3$
0.9–1.0	$(2.0\pm0.2)\times10^3$
1.0–1.1	$(1.1\pm0.1)\times10^3$
1.1–1.2	$(7.8\pm0.7)\times10^2$
1.2–1.3	$(4.6\pm0.4)\times10^2$
1.3–1.4	$(2.3\pm0.2)\times10^2$
1.4–1.5	$(1.5\pm0.1)\times10^2$
1.5–1.6	$(9.5\pm1.0)\times10^1$
1.6–1.7	$(6.1\pm0.8)\times10^1$
1.7–1.8	$(4.5\pm0.5)\times10^1$
1.8–1.9	$(3.1\pm0.3)\times10^1$
1.9–2.0	$(2.0\pm0.2)\times10^1$
2.0–2.1	$(1.2\pm0.2)\times10^1$
2.1–2.2	$(7.9\pm1.4)\times10^0$
2.2–2.3	$(5.8\pm0.9)\times10^0$
2.3–2.4	$(2.9\pm0.5)\times10^0$
2.4–2.5	$(2.4\pm0.4)\times10^0$
2.5–2.6	$(1.6\pm0.3)\times10^0$
2.6–2.7	$(1.2\pm0.2)\times10^0$
2.7–2.8	$(7.5\pm1.8)\times10^{-1}$
2.8–2.9	$(4.5\pm1.4)\times10^{-1}$
2.9–3.0	$(3.0\pm1.2)\times10^{-1}$
3.0–3.1	$(2.7\pm1.0)\times10^{-1}$
3.1–3.2	$(1.3\pm0.8)\times10^{-1}$
3.2–3.4	$(8.9\pm3.9)\times10^{-2}$
3.4–3.6	$(5.5\pm3.1)\times10^{-2}$

Table 4. Invariant cross-section for central 200 $A \cdot$GeV ^{16}O+Au collisions

p_T range (GeV/c)	$E(d^3\sigma/dp^3)$ (mb c^3 GeV^{-2})
0.4–0.5	$(3.0\pm0.7)\times10^4$
0.5–0.6	$(1.0\pm0.2)\times10^4$
0.6–0.7	$(5.5\pm0.7)\times10^3$
0.7–0.8	$(3.3\pm0.4)\times10^3$
0.8–0.9	$(2.0\pm0.2)\times10^3$
0.9–1.0	$(1.2\pm0.1)\times10^3$
1.0–1.1	$(7.9\pm0.8)\times10^2$
1.1–1.2	$(4.8\pm0.5)\times10^2$
1.2–1.3	$(3.1\pm0.3)\times10^2$
1.3–1.4	$(1.6\pm0.2)\times10^2$
1.4–1.5	$(1.0\pm0.1)\times10^2$
1.5–1.6	$(6.9\pm0.9)\times10^1$
1.6–1.7	$(5.0\pm0.7)\times10^1$
1.7–1.8	$(3.8\pm0.5)\times10^1$
1.8–1.9	$(2.5\pm0.3)\times10^1$
1.9–2.0	$(1.4\pm0.2)\times10^1$
2.0–2.1	$(9.6\pm1.5)\times10^0$
2.1–2.2	$(6.6\pm1.0)\times10^0$
2.2–2.3	$(4.5\pm0.7)\times10^0$
2.3–2.4	$(2.4\pm0.5)\times10^0$
2.4–2.5	$(1.9\pm0.4)\times10^0$
2.5–2.6	$(1.3\pm0.3)\times10^0$
2.6–2.7	$(6.5\pm0.3)\times10^{-1}$
2.7–2.8	$(5.3\pm2.3)\times10^{-1}$
2.8–3.0	$(3.6\pm1.3)\times10^{-1}$
3.0–3.2	$(1.7\pm0.8)\times10^{-1}$
3.2–3.6	$(4.6\pm2.7)\times10^{-2}$

Table 5. Invariant cross-section for peripheral 200 $A \cdot$GeV ^{16}O +Au collisions

p_T range (GeV/c)	$E(d^3\sigma/dp^3)$ (mb c^3 GeV^{-2})
0.4–0.5	$(6.1\pm1.5)\times10^3$
0.5–0.6	$(3.0\pm0.5)\times10^3$
0.6–0.7	$(1.4\pm0.2)\times10^3$
0.7–0.8	$(9.7\pm1.0)\times10^2$
0.8–0.9	$(5.8\pm0.6)\times10^2$
0.9–1.0	$(3.0\pm0.3)\times10^2$
1.0–1.1	$(1.6\pm0.2)\times10^2$
1.1–1.2	$(1.3\pm0.1)\times10^2$
1.2–1.3	$(7.9\pm1.0)\times10^1$
1.3–1.4	$(3.8\pm0.5)\times10^1$
1.4–1.5	$(2.1\pm0.3)\times10^1$
1.5–1.6	$(1.3\pm0.2)\times10^1$
1.6–1.7	$(6.6\pm1.3)\times10^0$
1.7–1.8	$(4.8\pm1.0)\times10^0$
1.8–1.9	$(3.5\pm0.6)\times10^0$
1.9–2.0	$(1.9\pm0.3)\times10^0$
2.0–2.2	$(1.1\pm0.2)\times10^0$
2.2–2.4	$(4.7\pm0.6)\times10^{-1}$
2.4–2.6	$(2.8\pm0.4)\times10^{-1}$
2.6–2.8	$(1.0\pm0.2)\times10^{-1}$

$\approx$1 GeV/c for p+p events is normalized to the π^0 data at $p_T=500$ MeV/c. The deviation between the experimental data and the exponential starting at about $p_T \approx 1.8$ GeV/c has been ascribed to hard scattering phenomena [14].

More insight into the particular mechanism of heavy-ion reactions at high energy can be gained by comparing central and peripheral ^{16}O+Au collisons with lighter systems. Collective effects or the formation of new states of nuclear matter are expected primarily in very central collisions. Data of peripheral collisions may provide, on the other hand, a link to p+nucleus and p+p reactions.

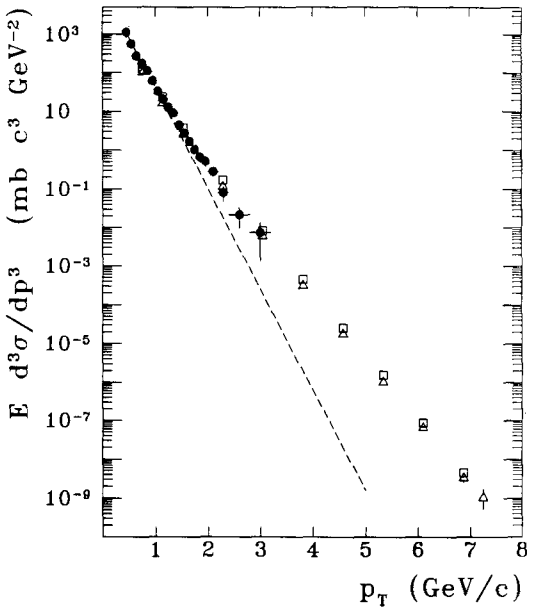

Fig. 8. Invariant π^0 cross sections from collisions of p projectiles with a Au target at 200 GeV measured in the pseudorapidity range $1.5 \leqq \eta \leqq 2.1$ (solid circles). Also shown are $\pi^\pm$ data for 200 GeV p+W reactions [13] (π^- = triangle, π^+ = square). For the exponential curve see the explanation in the text

In Fig. 9 invariant π^0 cross sections are plotted for minimum-bias events and in Fig. 10 for central and peripheral 200 $A \cdot$GeV ^{16}O+Au events. Attempts to fit the cross sections with a function consisting out of two thermal distributions do not give reliable results, i.e. the two temperatures depend on the relative normalization of the two thermal distributions and tend to be sensitive to statistical fluctuations [11]. Following a suggestion by Hagedorn [15], the $Ed^3\sigma/dp^3$-spectra are parameterized by the following expression:

$$E\frac{d^3\sigma}{dp^3} = \begin{cases} A\exp(-m_T/T) & \text{for } p_T \leqq 800.\text{MeV/c} \\ C\left(\dfrac{p_0}{p_T+p_0}\right)^n & \text{for } p_T \geqq 800.\text{MeV/c} \end{cases}, \tag{7}$$

where A, T, C, p_0 and n are parameters and m_T is the transverse mass ($m_T=\sqrt{p_T^2+m^2}$). The first expression is an approximation to a thermal distribution; the second is an empirical formula, inspired by QCD. The requirement that in both expressions the values and the slopes match at $p_T=0.8$ GeV/c leaves three free parameters, e.g. A, T, and n. The fit results are given in Table 6 and also shown in Figs. 9 and 10. Variations are found for the parameter n in Table 6, indicating that the spectra show different behaviours in the p_T range above 0.8 GeV/c. However, as already mentioned in [15], the parameters p_0 and n are highly correlated and hence no obvious interpretation can be given for n. Neverthe-

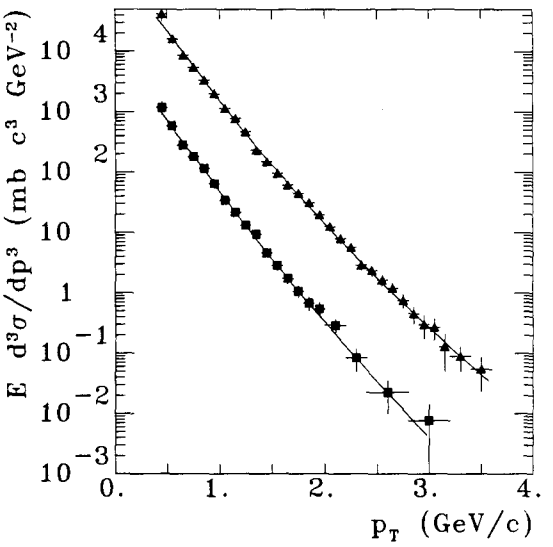

Fig. 9. Invariant π^0 cross sections from minimum-bias collisions of p (squares) and ^{16}O (triangles) projectiles with a Au target at 200 $A\cdot$GeV measured in the pseudorapidity range $1.5 \leqq \eta \leqq 2.1$. The lines represent fits to the data with (7) and parameters of Table 6

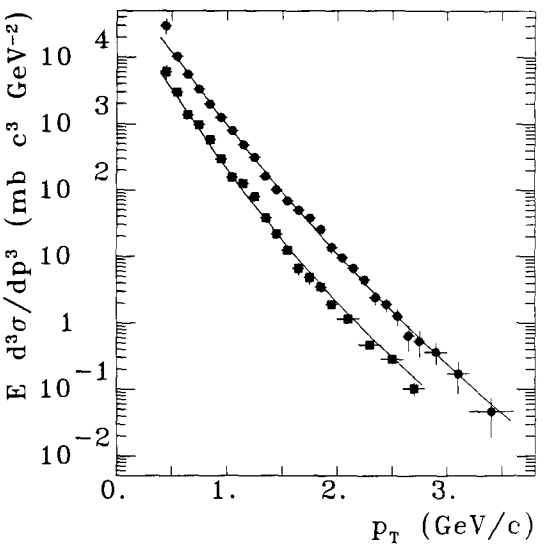

Fig. 10. Invariant π^0 cross sections from central (circles) and peripheral (squares) collisions of ^{16}O projectiles with a Au target at 200 $A\cdot$GeV measured in the pseudorapidity range $1.5 \leqq \eta \leqq 2.1$. The lines represent fits to the data with (7) and parameters of Table 6

Table 6. Parameters obtained from fitting (7) to the experimental data shown in Figs. 9 and 10. NDF is the abbreviation for the number of degrees of freedom

System	A (mb c^3 GeV^{-2})	T (MeV/c)	n	χ^2/NDF
200 GeV p+Au	$(1.3\pm0.5)\times10^4$	180 ± 16	37.6 ± 3.9	9.0/17
200 $A\cdot$GeV O+Au				
Minimum-bias	$(3.6\pm1.3)\times10^5$	184 ± 16	25.9 ± 2.4	17.8/27
Peripheral	$(6.6\pm2.9)\times10^4$	174 ± 18	16.8 ± 1.9	40.2/17
Central	$(1.7\pm0.8)\times10^5$	194 ± 22	26.0 ± 3.1	14.3/24

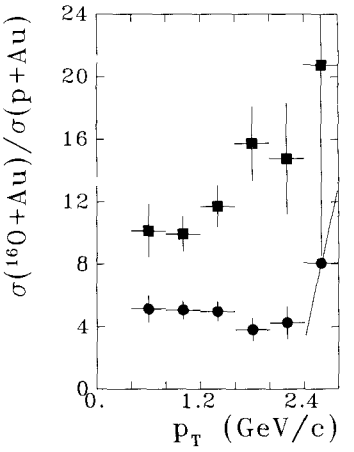

Fig. 11. Ratio of the π^0 spectra from central (squares) and peripheral (circles) $^{16}O+Au$ collisions normalized to the π^0 p_T spectra from minimum-bias p+Au events

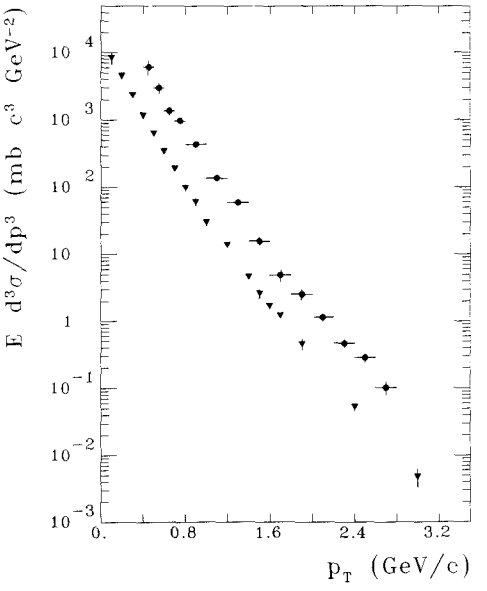

Fig. 12. Comparison of peripheral-collision π^0 spectra (circles) from the present $^{16}O+Au$ experiment at $\sqrt{s_{NN}} \cong 19.4$ GeV with charged-pion spectra from minimum-bias p+p data (triangles) at $\sqrt{s_{NN}} = 23$ GeV [17]. (π^- and π^+ data are averaged and plotted as a single set of data points which are scaled by a factor 100.)

less, for the parameter T no significant change for the different data sets is observed. As T also determines the mean transverse momentum this finding is consistent with results from [16], where nearly no variation of the mean transverse momentum for charged pions as a function of centrality and for different systems is found.

The difference between the $^{16}O+Au$ and p+Au spectra is more clearly displayed by plotting the ratios of the spectra (Fig. 11). A similar representation has previously been used by Cronin et al. [13] to discuss the *nuclear enhancement* of p+nucleus compared to p+p data. In that work, a scaling of the minimum-bias cross section ratios with $A^{\alpha}_{\text{target}}$ and a rise of α with p_T was observed for charged pions in the range 0.8 GeV/c $\leqq p_T$

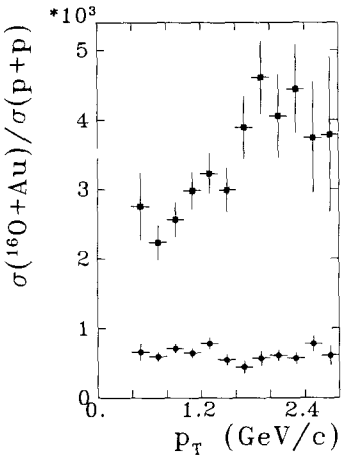

Fig. 13. Ratio of the π^0 p_T spectra from central (squares) and peripheral (circles) $^{16}O+Au$ collisions normalized to the $\pi^{\pm}$ spectrum from minimum-bias p+p events [17]

$\leqq 5$ GeV/c. A similar enhancement, which can be attributed to different projectile masses, is seen in going from p+Au to central $^{16}O+Au$ reactions, whereas the π^0 production from peripheral $^{16}O+Au$ reactions is very similar in shape to the π^0 production from p+Au events.

Fig. 12 shows a comparison of the peripheral-collision π^0 spectrum from $^{16}O+Au$ at 200 $A\cdot$GeV ($\sqrt{s_{NN}} \cong 19.4$ GeV) with charged-pion spectrum from inclusive p+p at $\sqrt{s_{NN}} = 23$ GeV [17]. There is a remarkable agreement in the spectral slope of the data up to the highest p_T of the present experiment. As mentioned before, the flattening in the p+p data beyond $p_T \approx 1.8$ GeV/c has been interpreted as the onset of hard QCD scattering, which becomes important for p_T values of several GeV/c (see Fig. 8). The similarity of the pion cross sections from peripheral $^{16}O+Au$ and p+p reactions and the difference between the π spectrum from central $^{16}O+Au$ and p+p events is even more pronounced by calculating ratios of the π spectra (see Fig. 13). As the charged pion spectra from [17] are binned differently than our π^0 cross sections, the $\pi^{\pm}$ data are fitted over the entire p_T range with the second function from (7) and then used to obtain Fig. 13. The ratio with central $^{16}O+Au$ data increases with p_T up to $p_T \approx 1.8$ GeV/c and becomes flat or even decreases at higher transverse momenta. The ratio is roughly constant for peripheral data. Therefore, it appears that the hard-scattering component of the elementary p+p interaction survives in peripheral heavy-ion collisions, but in the present p_T range it is strongly obscured by nuclear effects in central collisions. Forthcoming experiments in an extended p_T range are expected to reveal whether the hard component emerges in central collisions at higher p_T values.

The pattern of Fig. 13 is rather similar to results from pion measurements in p+p and $\alpha+\alpha$ experiments at $\sqrt{s_{NN}} = 63$ GeV and $\sqrt{s_{NN}} = 31.2$ GeV, respectively [14, 18, 19]. In these experiments a selection of the data was made according to their associated charged-particle multiplicities [14, 18], which corresponds to a certain energy in the ZDC in our experiment. Ratios between pion cross sections from events with high charged-particle multiplicities to those with low multiplicities show an increase by a factor of ≈ 2 when going from $p_T \approx 0.5$ GeV/c to $p_T \approx 2$ GeV/c, which is also observed in our data. The comparison between π spectra from $\alpha+\alpha$ and p+p events, which also means a comparison of events with different charged-particle multiplicities, shows the same behaviour below $p_T \approx 2$ GeV/c as mentioned before. At higher p_T values a flattening similar to that of Fig. 13 is found [19].

The observed similarity suggests a common underlying mechanism in p+p, $\alpha+\alpha$ and heavy-ion collisions, which causes the characteristic behaviour in different p_T regions. Especially the flattening above $p_T \approx 2$ GeV/c is interpreted in the framework of multiple-scattering of quarks and gluons [20]. For the p_T region <2 GeV/c several attempts have been made within hydrodynamical and thermodynamical models [21, 22] to describe the development of a hot and dense reaction zone and its connection to measured p_T spectra. In [23] a hydrodynamical model with isentropic expansion of a fireball and a certain freeze-out criterion is applied to our data. The low and intermediate part of the p_T spectrum is well described in this model with an initial energy density of 1.5–2 GeV/fm^3. However, the high p_T component in the peripheral-collision data is not described, indicating again that it may be due to hard scattering processes. In thermodynamical descriptions [24, 25], where the slopes of the p_T spectra are considered to be measures of the reaction temperature, different p_T regions and slopes are related to the breakup of substructures or to different scattering mechanisms. In the p_T region above 2 GeV/c, where hard QCD processes become increasingly important, the influence in the entrance channel may be studied by extending the comparison of p+p with heavy-ion data to mulitplicity selected spectra covering a large p_T range.

6 Summary

Transverse momentum distributions of π^0 have been measured for 200 $A\cdot$GeV p- and ^{16}O-induced reactions in the pseudorapidity range $1.5 \leqq \eta \leqq 2.1$. Centrality selection has been achieved by applying different cuts in the energy of the zero degree calorimeter (ZDC). The invariant π^0 cross sections have been fitted by a formula proposed by Hagedorn. In this model a temperature of ≈ 180 MeV/c is observed in the low p_T region for all spectra, indicating that the mean transverse momentum is rather constant as a function of the reaction centrality and of the projectile mass. Significant differences in the shape of the π^0 p_T distributions between central- and peripheral-$^{16}O+Au$ reactions have been observed. The variation is similar to the variation of charged pion p_T distributions from p+p and $\alpha+\alpha$ reactions at ISR energies. It is found that over the complete p_T range, the shape of the π^0 p_T distribution for peripheral events follows very closely the pion spectra from inclusive p+p collisions. A striking feature of the present $^{16}O+Au$ data

is that the onset of the hard-scattering component ($p_T > 1.8$ GeV/c) is not observed in the data for central collisions.

Acknowledgement. We thank P. Darriulat for illuminating discussions on the problem of overlapping photon showers. This work was partially supported by the West German BMFT and DFG, the VW-Stiftung, the United States DOE, the Swedish NFR, and the Alexander von Humboldt Foundation.

References

1. Quark Matter, H. Satz, H. Specht, R. Stock, (eds.): Z. Phys. C – Particles and Fields 38 (1988) and references therein
2. Quark matter formation and heavy ion collisions. Proc. Bielefeld Workshop (1982) M. Jacob, H. Satz (eds.) Singapore: World Scientific, 1982 and references therein
3. R. Albrecht et al. WA80 Coll.: Phys. Lett. B201 (1988) 390 H. Löhner et al. WA80 Coll.: Z. Phys. C – Particles and Fields 38 (1988) 97
4. H.H. Gutbrod et al.: GSI preprint GSI-85-32, 1985; CERN SPSC/85-39/M406
5. R. Albrecht et al. WA80 Coll.: Phys. Lett. B199 (1987) 297
6. R. Albrecht et al. WA80 Coll.: Phys. Lett B202 (1988) 596
7. H. Baumeister et al.: Design and performance of the SAPHIR lead glass calorimeter. Nucl. Instrum. Methods (to appear)
8. M. Della Negra: Phys. Scr. 23 (1981) 469
9. P.R. Bevington: Data reduction and error analysis for the physical sciences. New York: McGraw-Hill 1969
10. S.P. Sørensen et al. WA80 Coll.: Z. Phys. C – Particles and Fields 38 (1988) 3
11. L. Dragon: Doctoral thesis, University of Münster (1989)
12. B. Andersson, G. Gustafson, B. Nilsson-Almqvist: Nucl. Phys. B281 (1987) 289; B. Nilsson-Almqvist, E. Stenlund: Comp. Phys. Commun. 43 (1987) 387
13. J.W. Cronin et al.: Phys. Rev. D11 (1975) 3105; D. Antreasyan et al.: R.L. Summer: Phys. Rev. D19 (1979) 764
14. M.A. Faessler: Phys. Rep. 115 (1984) 1
15. R. Hagedorn: Riv. Nuovo Cimento 6 (1983) 1
16. T. Åkesson et al. HELIOS Coll. Z. Phys. C – Particles and Fields 46 (1990) 361
17. B. Alper et al. BS Coll.: Nucl. Phys. B100 (1975) 237
18. W. Bell et al. CERN-Heidelberg-Lund Coll.: Z. Phys. C – Particles and Fields 27 (1985) 191
19. T. Åkesson et al. AFS Coll.: Nucl. Phys. B209 (1982) 309–320
20. M. Lev, B. Petersson: Z. Phys. C21 (1983) 155; U.P. Sukhatme, G. Wilk: Phys. Rev. D25 (1982) 1978
21. M. Kataja, P.V. Ruuskanen, L.D. McLerran, H. von Gersdorff: Phys. Rev. D34 (1986) 2755
22. M. Danos, J. Rafelski: Phys. Rev. D27 (1983) 671
23. K.S. Lee, U. Heinz: Z. Phys. C – Particles and Fields 43 (1989) 425
24. E.V. Shuryak: Phys. Rep. 61 (1980) 71
25. E.V. Shuryak: Novosibirsk, preprint 87–142; E.V. Shuryak: Phys. Lett. B207 (1988) 345; E.V. Shuryak: CERN-TH-5386/89 (1989), to be published in L. van Hove Festschrift, World Scientific